EVALUATION OF THE THERMAL CONDUCTIVITY OF FROST FORMED ON PARALLEL PLATE CHANNELS

Silvia Negrelli, silvia.negrelli@ufpr.br
Valter S. Nascimento Jr
Christian J. L. Hermes
Laboratory of Thermodynamics and Thermophysics, Department of Mechanical Engineering, Federal University of Paraná, 89531990 Curitiba-PR, Brazil.

Abstract. *Computational models used to predict the growth of a frost layer are usually based on the fundamental principles of Thermodynamics and Transport Phenomena. However, those models rely on empirical correlations to compute the thermophysical properties of the frosted medium, particularly the density and the effective thermal conductivity. A literature review shows that the open literature lacks of a physically-based model for the thermal conductivity of frost formed in different operating conditions. Therefore, the present study is aimed at investigating, by means of an experimental approach, the frost growth process on parallel plate channels and the influence of the key parameters on the effective thermal conductivity of frost. A theoretical analysis was conducted based on the limiting cases of serial and parallel association of the thermal resistances of moist air and ice crystals, thus setting the theoretical background for a dimensionless model for the thermal conductivity as a function of the porosity of the frosted medium. The experimental work was carried out by means of a closed-loop wind-tunnel facility, which provides a strict control of the psychrometric conditions at the entrance of the test section as well as the plate surface temperatures. A dataset comprising of 45 experimental points was gathered in order to come up with a semi-empirical correlation for the thermal conductivity of frost as a function of the frost porosity and the surface temperature. The correlation is able to predict ~90% of the experimental data points within the ±15% thresholds*

Keywords: *frost, thermal conductivity, density, semi-empirical correlation, experimental work, plate channels*

1. NOMENCLATURE

Roman

As	Surface area, m²
a, b	Coefficients of equations (11) and (12)
C	Coefficient of equation (1)
c_p	Specific heat, kJ kg-1K-1
h	Heat transfer coefficient, W m^{-2} K^{-1}
h_m	Mass transfer coefficient, kg m^{-2} K^{-1}
i_{sv}	Latent heat of sublimation, kJ kg^{-1}
k	Thermal conductivity , W m^{-1} K^{-1}
Le	Lewis number, Le = α/D
M	Mass, kg
m	Mass flux, kg m-2 s^{-1}
Nu	Nusselt number, Nu = hL/k
Pr	Prandtl number, Pr = ν/α
q	Heat flux, W m^{-2}
RT	Thermal resistance, m^2 K W^{-1}
Sc	Schmidt number, Sc = ν/D
Sh	Sherwood number, Sh = h_mL/D
t	Time, s
T	Temperature, K

Greek

ρ	Density, kg m^{-3}
ε	Frost porosity
δ	Thickness, m
Λ	Modified Jakob number
φ	Relative humidity
ω	Humidity ratio, kg_v kg_a^{-1}

Subscripts

a	Moist air
dew	Dew-point
f	Frost
g	Geometric mean
i	Ice
lat	Latent
p	Parallel association
s	Serial association
sat	Saturation
sen	Sensible
w	Wall surface

2. INTRODUCTION

Frost is a porous medium comprised of ice crystals and moist air, being formed by the ablimation of water vapor present in the air stream. It often builds-up on evaporators of refrigeration systems, resulting in an increased energy input to accomplish the same refrigerant effect. To mitigate these undesired effects, many efforts have been done aiming at simulating the frost growing process on flat surfaces (Hermes et al., 2009; Hermes, 2012) and parallel plate channels (Loyola et al., 2014). Most models, however, rely on empirical correlations to compute the termophysical properties of the frosted media, particularly the frost density (or porosity) and the effective thermal conductivity, which limits their applications to narrow ranges of frost morphologies.

Studies of the frost density have been successfully carried out to come up with a semi-empirical correlation which is valid for a wide frost morphology span. For instance, Hermes et al. (2014) and Nascimento et al. (2015) proposed the

following semi-empirical correlation for the density of frost formed on flat plates and parallel plate channels, respectively:

$$\frac{\rho_f}{\rho_i} = C\,\Lambda^{-n}\sqrt{t} \tag{1}$$

where n=3/2 and C=0.0024 for flat surfaces and n=3/4 and C=0.0022 for parallel plate channels, ρ_i and ρ_f are densities of ice and frost in [kg m^{-3}], respectively, and t is time in [s]. In addition, Λ is the modified Jakob number introduced by Hermes et al. (2014) as follows:

$$\Lambda = \frac{c_p(T_{dew} - T_w)}{i_{sv}(\omega_a - \omega_{sat}(T_w))} \tag{2}$$

where c_p is the specific heat of moist air, T_{dew} is the dew-point temperature, i_{sv} is the latent heat of ablimation, ω_a is the humidity ratio of the air, and $\omega_{sa}t(T_w)$ is the humidity ratio of the saturated air at the wall temperature. It is worthwhile noting that such a correlation was derived based on the fact that the frost thickness, δ_f, follows the $\sqrt{t}$ scale, so does the frost density, ρ_f, in such a way that the frost mass has a nearly linear dependence with time, since $M \sim \rho_f\delta_f \sim \sqrt{t}\sqrt{t} \sim t$.

An inspection of the open literature conducted in a prior work (Negrelli and Hermes, 2015) revealed that there was an opportunity for a physically-based model for the thermal conductivity of frost. Negrelli and Hermes (2015) then came up with a semi-empirical correlation for the thermal conductivity of frost as a function of frost porosity and wall temperature, based on experimental data points for flat surfaces collected from the literature.

Nevertheless, only one record was found in the literature with regard to the thermal conductivity of frost formed on parallel plate channels (Ostin and Andersson, 1990). Their study, however, correlates the thermal conductivity as an empirical function of the frost density only, which shows errors up to 50%. Therefore, a review of the state-of-the-art also reveals that the literature lacks of a physically-consistent model for the thermal conductivity of frost built-up on parallel plate. The present paper is aimed at accomplishing this task.

3. EXPERIMENTAL WORK

3.1 Test rig

The testing facility is a closed-loop wind-tunnel facility, as depicted in Figure 1. The apparatus allows a strict control of the psychrometric conditions of the air, the air velocity and the plate temperature. The wind-tunnel has a 200 x 200 mm cross section and its walls are made of 50-mm thick EPS plates sandwiched between 20-mm thick plastic liners so as to provide structural resistance.

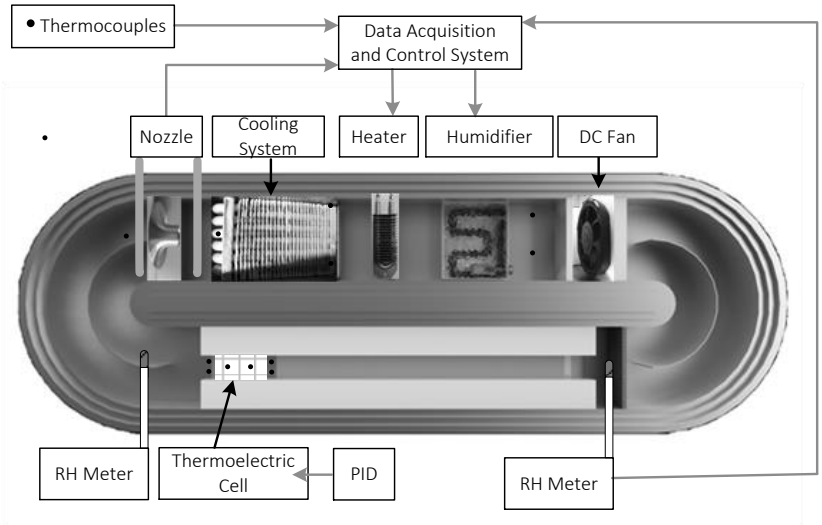

Figure 1. Schematic representation of the closed-loop wind-tunnel facility

The air-loop is comprised of two straight sections and two return bends. One side contains the ½" and 1" nozzles for air flow measurements, an evaporator coil for cooling and dehumidifying the air stream, and two PID-driven electric heaters, a finned 350-W one for regulating the air temperature and a coiled 180-W one immersed in a humidifying tray

for controlling the air humidity. A DC fan is also used to set the air velocity at the test section. The air flow rate was measured using a differential pressure transducer ranging from 0 to 125 Pa with an uncertainty of 0.25% (full-scale).

On the other side, there is an EPS-insulated 1.0-m long straight channel, which ensures the proper thermal-fluid-dynamic development, and the test section itself, which is comprised of two PID controlled thermoelectric devices. The test section is comprised of two T-shaped aluminum blocks, whose bigger ends (L=120 mm x W=60 mm) are connected to the thermoelectric cells located at the outer side of the wind-tunnel walls to promote the heat dissipation from the hot ends. The smaller ends (L=40 mm x W=60 mm) form the parallel plate channel where frost builds-up.

The test section, i.e. the channel, is formed by two parallel 3-mm thick copper plates placed at the top of the aluminum blocks. Two thermocouples and a heat flux sensor (±5 W/m² uncertainty) were embedded into the plate for the sake of temperature and heat flux measurements, respectively. Four T-type thermocouples (±0.2 K uncertainty) were located at the test section entrance (2) and exit (2) ports, being the upstream ones responsible for controlling the 350-W heater. A square 22-mm sided triple-layer glass window is located in front of the test section to allow visualization. A stereoscopic device, with a 3 megapixel 10x ocular lens and 0.5x photographic lens camera, was used to take pictures of the frost layer during the test. The illumination was provided by optical fibers. The frost thickness was measured from the images with a ±50 μm uncertainty.

A homogenizer was placed at the channel inlet to promote flow laminarization. A capacitive relative humidity transducer (±2% uncertainty) was installed at the channel inlet to control the inflow air humidity by means of the 180-W heater. Additional thermocouples were installed at the nozzle and at the surrounding air. The room temperature was kept at 20°C ± 2°C by an on-off controlled air conditioner.

3.2 Test procedure and data processing

Before starting a particular test, all variables must achieve steady-state conditions. To avoid frost formation during the transient regime, a by-pass system was adopted, which consists of a manual damper that diverts the air flow from the test section, so that the cold surfaces are not exposed to the moist air stream. During the test, pictures of the test section are taken at every minute. The images were then processed to come out with the time-evolution of the frost thickness, δ_f. The frost mass, M, was measured afterwards by a high-precision scale with ±0.01 g uncertainty. The frost density was then calculated from:

$$\rho_f = \frac{M}{A_s\left(\delta_{f,top} + \delta_{f,bottom}\right)} \tag{3}$$

where A_s is the surface area. Since the frost mass varies linearly with time (Nascimento et al, 2015), the mass flux of water vapor transferred to the surface m can be calculated from:

$$m = \frac{M}{A_s t} \tag{4}$$

where t is the total time duration of the test. During the test, the mass and heat transports are regarded as quasi-steady one-dimensional processes (Hermes, 2012), and the heat conduction is modeled using resistance association, as shown in Figure 2.

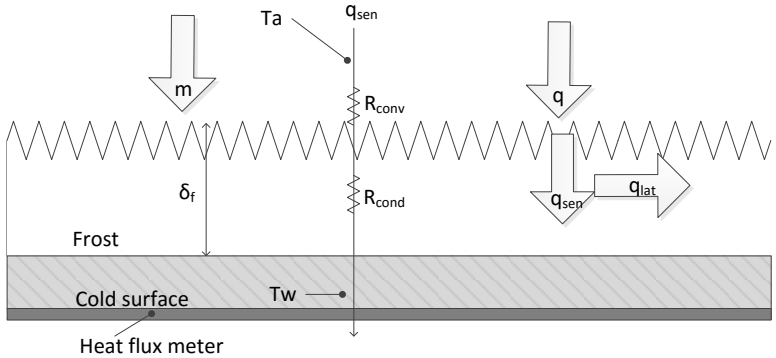

Figure 2. Schematic representation of the heat flux through the frost layer

The total heat flux measured by the heat flux meter is the sum of the latent heat flux (q_{lat}) and the sensible heat flux (q_{sen}). The former can be evaluated from:

$$q_{lat} = mi_{sv} \tag{5}$$

Once the air and the wall temperatures are known, the sensible heat flux term can be evaluated from:

$$q_{sen} = \frac{T_a - T_w}{R_T} \tag{6}$$

where T_a is the air temperature, T_w is the wall temperature, and R_T is an overall thermal resistance to sensible heat transfer, comprised of the convective (1/h) and the conductive (δ_f/k_f) parts, and calculated from:

$$R_T = \frac{1}{h} + \frac{\delta_f}{k_f} \tag{7}$$

where δ_f is the frost thickness, k_f is the effective thermal conductivity of frost, and h is the heat transfer coefficient, calculated from the mass transfer coefficient h_m through the so-called Lewis boundary layer analogy, $Nu/Pr^{1/3}=Sh/Sc^{1/3}$ (Baehr and Stephan, 2006), thus yielding:

$$h = h_m c_p Le^{2/3} \tag{8}$$

where Nu and Sh are the Nusselt and Sherwood numbers, respectively, Pr and Sc are the Prandtl and Schmidt numbers, respectively, and $Le=Sc/Pr=\alpha/D$ is the Lewis number. The mass transfer coefficient, on the other hand, can be obtained from:

$$h_m = \frac{m}{\omega_a - \omega_{sat}(T_w)} \tag{9}$$

Therefore, equation (6) and (7) can be combined and re-written in the following form, which allows the straightforward computation of the effective thermal conductivity of the frost layer:

$$k_f = \frac{q_{sen}\delta_f h}{(T_a - T_w)h - q_{sen}} \tag{10}$$

3.3 Test planning

As shown in Negrelli and Hermes (2015), the key parameters that affect the thermal conductivity of frost are the porosity and the wall temperature, which were therefore selected as the independent variables of the experiment. The temperature levels were chosen to span a wide range of frost morphologies, -23, -15 and -7°C, representing the shapes of columns, plates and columns, respectively, according to the Kobayashi's (1958) morphology map.

The test conditions were selected to cover a wide range of porosities, expressed in the form of the modified Jakob number, Λ, which incorporates the key operating conditions that affect the frost density, as shown in equation (1). Therefore, the test plan comprises three levels of temperature and three levels of Λ for each temperature, as summarized in Table 1. Five different experiments were conducted for each test condition, each one lasting a different time duration, so that different densities (porosities) could be achieved (see equation 1).

Table 1. Summary of the test conditions

#	T_w (°C)	T_a (°C)	φ_a	Λ
1	-23	-3.5	80	2.907
2	-23	-1	80	2.386
3	-23	5	80	1.948
4	-15	4	75	1.703
5	-15	10	80	1.275
6	-15	15	80	1.118
7	-7	5	70	1.396
8	-7	10	75	1.072
9	-7	15	80	0.958

3.4 Data correlation

The effective thermal conductivity of porous media depends on the thermal conductivities of each phase (solid and fluid), on the volume fraction between the fluid phase and the porous medium (i.e., porosity), and on the array formed by particles and pores. In high porosities, the thermal conductivity of frost approaches that of moist air (k_a ~ 0.02 W $m^{-1}K^{-1}$), and for low porosities, it approaches that of ice (k_i ~ 2.0 W $m^{-1}K^{-1}$). The crystal array also influences the thermal conductivity, which is dictated by the frost morphology that in turn depends on the surface temperature and the supersaturation degree. Two common frost morphologies are formed, providing two limiting cases for thermal resistance association, parallel and serial. In general, porous media are not well represented by only one of the two structures, and the effective thermal conductivity has an intermediate figure. Nield and Bejan (2006) proposed the geometric mean (k_g), that is appropriate for most porous media. Negrelli and Hermes (2015) adapted equation (14) for frosted media by making $k_f=k_g$, dividing by k_i, taking the logarithm in both sides, and adding two linear coefficients (slope and interception) to come out with

$$\frac{k_f}{k_i} = a\left(\frac{k_a}{k_i}\right)^{b\varepsilon} \tag{11}$$

where coefficients "a" and "b" must be best fitted to the experimental data for different temperature ranges, which depend on the surface temperature, and ε is the porosity, calculated from:

$$\varepsilon = \frac{\rho_i - \rho_f}{\rho_i - \rho_a} \tag{12}$$

where ρ_a and ρ_i are the densities of moist air and ice, respectively.

5. RESULTS

Since equation (12) is a function of the porosity only, three different curves were fitted to the experimental data obtained in-house, one for each temperature. Three pairs of coefficients "a" and "b" were then obtained by means of the least-squares method, one for each temperature as summarized in Table 2.

Table 2. Coefficients of equation (11) and (12)

T_w (ºC)	Morphology	Interception (a)	Slope (b)	RMS Error
-23°C	Needles and sheaths	1.321	0.858	0.090
-15°C	Plates and dendrites	2.102	0.927	0.120
-7°C	Sheaths	1.769	0.834	0.132

The results were plotted in a dimensionless chart introduced by Negrelli and Hermes (2015), where one can see that k_p is the maximum allowed thermal conductivity, whereas k_s is the minimum one. The geometric mean provides intermediate values between k_s and k_p. Figure 3 shows the fitting results for the three temperatures, where one can observe that equation (16) is able to predict the experimental trends quite satisfactorily.

Also, it can be observed that higher temperatures lead to higher thermal conductivities due to the combination of two effects: higher thermal conductivity of ice and air (minor effect) and higher mass diffusion through frost layer (major effect). The frost morphology has not affected the thermal conductivity too significantly. For the intermediate temperature (-15°C), frost is supposed to grow according to a plate-shaped morphology, so that the thermal conductivity is expected to be lower. Nevertheless, after the initial stages of growing, new molecules of vapor start to diffuse through the frost layer, so that the diffusion transport happens to be more influential than that of the morphology. For the temperatures of -23°C and -7°C, frost is supposed to grow as columns, reason why the two curves are nearly parallel.

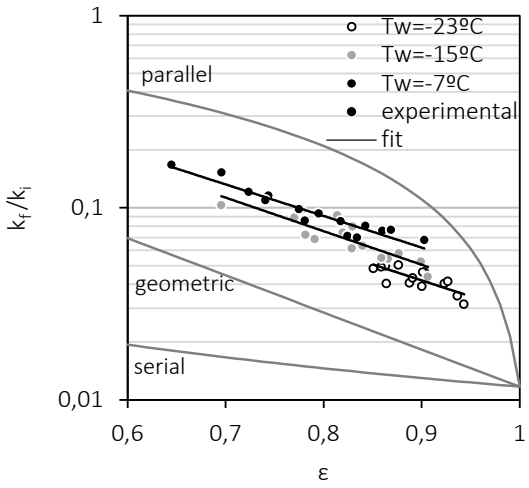

Figure 3. Best fitting of equation (16) spanning three different temperatures: -23°C, -15°C and -7°C

Figure 4 presents a comparison between the experimental data for the thermal conductivity of frost and the figures predicted by the equation (16), where it can be seen that 42 out of 45 data points (~90%) lay within the 15% thresholds. The error bars indicate the propagated uncertainties observed in case when equation (16) is fed with experimental values for the temperature and humidity. The maximum figures have not exceeded the ±15% thresholds.

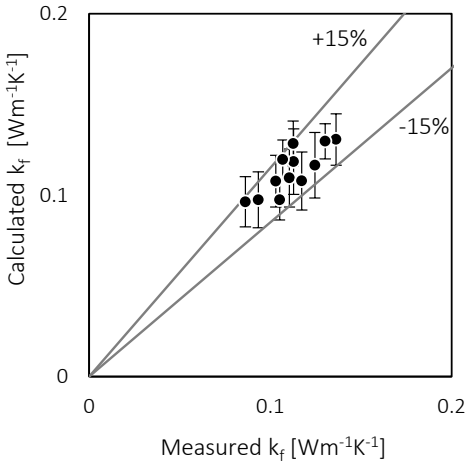

Figure 4. Comparison between experimental and predicted thermal conductivity of frost using data from tests #1 to #9

6. CONCLUSIONS

The present paper presented an experimental analysis of the thermal conductivity of the porous medium formed by ice crystals on moist air carried out by means of a purpose-built closed-loop wind-tunnel facility, which provides a strict control of the psychrometric conditions at the entrance of the test section as well as of its surface temperatures. A semi-empirical correlation for the thermal conductivity of frost formed on parallel plate channel was put forward based on 45 data points spanning different wall temperatures and frost porosities, being able to predict 42 out of 45 data points (~90%) within the ±15% error bounds.

7. ACKNOWLEDGEMENTS

This work was carried out under the auspices of the Brazilian Government funding agency CNPq (Grant No. 441603/2014-9). Ms. S. Negrelli and Mr. V. S. Nascimento Jr duly acknowledged the CAPES Agency, Government of Brazil, for supporting their post-grad education at the Federal University of Paraná.

8. REFERENCES

Auracher H, Effective thermal conductivity of frost, Proceedings of the International Symposium of Heat and Mass Transfer in Refrigeration Cryogenics, Dubrovnik (1986) 285-302

Baehr HD, Stephan K, Heat and Mass Transfer, second ed., Springer, Berlin, Germany, 2006.
Brian PLT, Reid RC, Brazinsky I, Cryogenic frost properties, Cryogenic Technology 10/11 (1969) 205-212
Hermes CJL, An analytical solution to the problem of frost growth and densification on flat surfaces, Int. J. Heat and Mass Transfer 55 (2012) 7346–7351
Hermes CJL, Loyola FR, Nascimento VS, A semi-empirical correlation for the frost density, Int. J. Refrigeration 46 (2014) 100-104
Hermes CJL, Piucco RO, Melo C, Barbosa Jr. JR, A study of frost growth and densification on flat surfaces, Exp. Therm. Fl. Sci. 33 (2009) 371-379
Knabben FT, Hermes CJL, Melo C, In-situ study of frosting and defrosting processes in tube-fin evaporators of household refrigerating appliances, Int. J. Refrigeration 34 (2011) 2031-2041.
Kobayashi T, On the habit of snow crystals artificially produced at low pressures, J. Met. Soc. Japan 36 (1958) 193-208
Loyola FR, Nascimento VS, Hermes CJL, Modeling of frost build-up on parallel-plate channels under supersaturated air-frost interface conditions, Int. J. Heat and Mass Transfer 79 (2014) 790-795
Na B, Webb RL, New model for frost growth rate, Int. J. Heat Mass Transfer 47 (2004) 925-936
Nascimento VS, Loyola FR, Hermes CJL, A study of frost build-up on parallel plate channels, Exp. Therm. Fl. Sci. 60 (2015) 328-336
Negrelli S, Hermes CJ, A semi-empirical correlation for the thermal conductivity of frost. Int. J. Refrigeration 58 (2015) 243-252
Nield DA, Bejan A, Convection in Porous Media, Springer, 2006
Ostin R, Andersson S, Frost growth parameters in a forced air stream, Int. J. of Heat Mass Transfer 34 (1991) 1009-1017
Pitman D, Zuckerman B, Effective thermal conductivity of snow at -88°, -27°, and -5°C, J. Applied Physics 38 (1967) 2698-2699
Ribeiro RS, Hermes CJL, Algebraic modeling and thermodynamic design of fan-supplied tube-fin evaporators running under frosting conditions, Applied Thermal Engineering 70 (2014) 552-559
Silva DL, Hermes CJL, Melo C, First-principles simulation of frost accumulation on fan-supplied tube-fin evaporators, App. Therm. Eng. 31 (2011) 2616-2621